HHS Public Access

Author manuscript

Neuron. Author manuscript; available in PMC 2017 April 06.

Published in final edited form as:

Neuron. 2016 April 6; 90(1): 86–100. doi:10.1016/j.neuron.2016.02.037.

Cooperative subnetworks of molecularly-similar interneurons in mouse neocortex

Mahesh M Karnani[1], **Jesse Jackson**[1], **Inbal Ayzenshtat**[1], **Jason Tucciarone**[2], **Kasra Manoocheri**[1], **William G Snider**[1], and **Rafael Yuste**[1]

[1]Neurotechnology Center, Department of Biological Sciences, Columbia University, New York, NY 10027

[2]Cold Spring Harbor Laboratory, Cold Spring Harbor, New York 11724, MSTP/Neuroscience Graduate Program, Stony Brook University, Stony Brook, New York 11790

Summary

Simultaneous co-activation of neocortical neurons is likely critical for brain computations ranging from perception and motor control to memory and cognition. While co-activation of excitatory principal cells (PCs) during ongoing activity has been extensively studied, that of inhibitory interneurons (INs) has received little attention. Here we show *in vivo* and *in vitro* that members of two non-overlapping neocortical IN populations, expressing somatostatin (SOM) or vasoactive intestinal peptide (VIP), are active as populations rather than individually. We demonstrate a variety of synergistic mechanisms, involving population-specific local excitation, GABAergic disinhibition and excitation through electrical coupling, which likely underlie IN population co-activity. Firing of a few SOM or VIP INs recruits additional members within the cell type via GABAergic and cholinergic mechanisms, thereby amplifying the output of the population as a whole. Our data suggest that IN populations work as cooperative units, thus generating an amplifying nonlinearity in their circuit output.

Introduction

Neuronal activity in the neocortex is organized to form groups of simultaneously active (co-active) cells termed ensembles (Harris, 2005, Miller et al., 2014). These co-active ensembles encode information in neuronal processes ranging from memory to innate behavior (Cowansage et al., 2014, Root et al., 2014, Hebb, 1949). Co-activation of neurons inevitably depends on synaptic connectivity of excitatory as well as inhibitory neurons, but while co-activity of neocortical principal cells (PCs) has been studied extensively (Ch'ng and Reid,

Corresponding author: Mahesh Karnani, miikael.mmk@gmail.com.

Author contributions

Performed experiments: MMK (in vitro), JJ (in vivo), JT (tracing). Designed experiments: MMK, JJ. Analysis and software: MMK, JJ, IA, KM, WGS. Funding acquisition and resources: RY. Wrote paper: MMK, JJ, IA with input from all authors.

2010, Miller et al., 2014, Bathellier et al., 2012, Sakata and Harris, 2009), that of inhibitory interneurons (INs) has received little attention.

In particular, population patterns of cortical activity during sensory stimulation and in its absence (ongoing activity) are surprisingly similar for excitatory neurons (Ch'ng and Reid, 2010, Miller et al., 2014, Sakata and Harris, 2009, Gentet et al., 2012, Ji and Wilson, 2007, Luczak et al., 2009). The visual stimulus responses of multiple IN types have been probed (Hofer et al., 2011, Kerlin et al., 2010, Sohya et al., 2007, Cottam et al., 2013, Runyan et al., 2010) and their overall lack of selectivity suggests broad co-activation of INs also during ongoing activity. Yet, the function of only one IN subpopulation, parvalbumin expressing INs (PVs), has been studied during ongoing activity (Hofer et al., 2011). It is important to study co-activity patterns of other INs during ongoing activity, as it reflects flow of information through the cortical circuit without sensory driven thalamocortical input and is therefore the optimal situation to assess 'spontaneously' generated co-activity of INs. Furthermore, ongoing activity is thought to be involved in memory replay and intrinsic mental states (Ch'ng and Reid, 2010, Miller et al., 2014, Sakata and Harris, 2009, Gentet et al., 2012, Ji and Wilson, 2007, Luczak et al., 2009).

PVs, together with somatostatin expressing cells (SOMs) and vasoactive intestinal peptide expressing cells (VIPs) form three non-overlapping populations that account for ~85% of neocortical INs (Rudy et al., 2011), and have partially dissociable roles in neural computations (Fu et al., 2014, Lee et al., 2013, Lee et al., 2012, Pi et al., 2013, Zhang et al., 2014). The inhibitory connectivity of PVs, SOMs and VIPs was recently described by optogenetically activating one population at a time (Lee et al., 2013, Pfeffer et al., 2013, Pi et al., 2013) leading to a prevailing model of hierarchical disinhibitory motifs (Hangya et al., 2014, Harris and Shepherd, 2015, Kepecs and Fishell, 2014). However, it is unclear how interneurons coordinate their activity within subpopulations. It is particularly puzzling how mutually inhibitory interneuron populations manage to operate together while embedded within a highly interconnected network. Indeed, while it is firmly established that nearby PCs excite PVs and SOMs with population-specific synaptic dynamics (Beierlein et al., 2003, Reyes et al., 1998, Silberberg and Markram, 2007, Kapfer et al., 2007), the local excitatory connections driving VIPs have remained poorly studied as recent studies suggest that VIPs specialize in receiving long-range excitation (Fu et al., 2014, Lee et al., 2013, Zhang et al., 2014).

Here we show that the neocortex has several complementary and overlapping mechanisms that can promote coordinated firing within genetically defined interneuron populations. First, we demonstrate within-population co-activity of both SOMs and VIPs in vivo using 2-photon calcium imaging. Secondly, we show that nearby PCs excite SOMs and VIPs with different synaptic dynamics and that VIPs and SOMs receive local excitation from separate subnetworks of PCs. We show that the specific pattern of electrical and inhibitory connectivity among VIPs, SOMs and PVs can mediate population co-activity. Finally, we show that the firing of a small fraction of the SOM or VIP population is sufficient to recruit other neurons in the same cell class, thereby demonstrating a circuit mechanism of interneuron excitation. Collectively, these data demonstrate that neocortical interneuron populations have multiple specializations that can promote within-population co-activity.

Results

VIP and SOM interneuron populations are co-active in vivo

We first investigated spontaneous activity patterns of VIPs and SOMs by recording ongoing activity while mice were awake in a dark room. We used 2-photon Ca^{2+} imaging through a thinned skull in primary visual cortex (V1) of VIP-cre: :LSL-TOM and SOM-cre: :LSL-TOM mice injected with AAV1-syn-GCAMP6s (Figure 1). Both VIPs and SOMs were co-active with their population members (Figure 1A,B,E,F; Movies S1 and S2). Since activity of VIPs and SOMs is modulated by animal movement (Fu et al., 2014, Polack et al., 2013), we divided the data into 'stationary' and 'locomotion' epochs measured by monitoring movement of the running disk the mice were on. During both epochs and across 11 movies from 5 animals (5–19 VIPs and 41–137 Non-VIPs per movie), VIP pairs had higher pairwise correlation coefficients than non-VIP pairs or VIP/non-VIP pairs (Figure 1C,D, statistics in figure legends). To avoid potential systematic biases in the ΔF/F correlations, we repeated the analyses with binarized data (see Methods) and obtained similar results (Figure 1C,D). We performed the same analyses on 8 movies from 4 SOM-cre: :LSL-TOM mice (4–12 SOMs and 39–75 Non-SOMs per movie) and found that SOMs are also co-active together (Figure 1G,H). We further analyzed the movies with highest amounts of GCAMP-expressing and active INs by counting how many INs were active together in the same frame in binarized data. This analysis also indicated that VIPs and SOMs are more co-active than shuffled surrogate data, or the other cells in the imaged region (Figure S1). Locomotion increased the pairwise correlations within both VIP (stationary $R = 0.07 \pm 0.01$, locomotion $R = 0.13 \pm 0.03$, $P = 0.038$) and SOM populations (stationary $R = 0.13 \pm 0.04$, locomotion $R = 0.22 \pm 0.04$, $P = 0.005$), consistent with increased neuronal activity during animal movement. Together these data demonstrate that VIPs and SOMs tend to be active together with their population members during ongoing neuronal activity. Therefore, we next went on to study the underpinnings of within population co-activity in slices using electrophysiology.

Layer 2/3 PCs innervate VIPs and SOMs with different input dynamics

It has been suggested that VIPs and SOMs might receive unspecific excitatory input from surrounding PCs (Kerlin et al., 2010) similarly to PVs (Hofer et al., 2011). To probe this directly, we used multi-cell patch clamp to assess connectivity parameters between nearby (intersomatic distances 20–100 μm) PCs and VIPs or SOMs in triple-transgenic VIP-cre: :LSL-TOM: :SOM-GFP(GIN) slices (see Methods). PCs formed excitatory synapses onto VIPs and SOMs at similar rates, but synapses onto VIPs were depressing, while those onto SOMs were facilitating (Figure 2A). Additional recordings in primary somatosensory cortex (S1) also demonstrated a depressing synaptic PC->VIP connection (5/38 connections, 13%) suggesting that the organization of SOM versus VIP excitation dynamics is conserved across sensory cortices. The differences in excitatory input dynamics suggest that VIPs and SOMs will be active at different times during excitatory afferent drive of these circuits.

To see whether these dynamics have an impact when the whole microcircuit is activated, we elicited network activation in slice by a broad optogenetic activation (Figure 2B). We expressed the excitatory opsin C1V1 under the CaMKIIα promoter (CaMKIIα-C1V1(E162T)-p2A-EYFP) to direct it mostly to PCs (Coultrap and Bayer, 2012, Packer et

al., 2012) in VIP-cre: :LSL-TOM: :SOM-GFP(GIN) animals. We then patched a VIP and a SOM (at 50–150 μm intersomatic distance) and activated the circuit with a continuous 0.5 s pulse of green light (Figure 2B). The light stimulus recruited sustained 22 ± 8 Hz firing in 50% of PCs recorded in the same preparations for calibration (Figure 2B). VIPs and SOMs were recruited in a highly stereotyped manner during optogenetic activation; VIPs tended to fire a single AP in the beginning of the 0.5 s light pulse, followed by quiescence, while SOMs ramped up to an average firing rate of 26 ± 7 Hz during the pulse (Figure 2B). This broad activation of the local microcircuit includes axon terminals expressing C1V1, therefore these results may be due to multiple complex network interactions among the excitatory and inhibitory cell types. To better characterize the cellular elements stimulated by light under these conditions, we also recorded from PVs in PV-cre: :LSL-TOM animals and found that 65% (11/17) of PVs were recruited to a sustained firing at 46 ± 9 Hz by the light step. Thus, under this broad excitation of inhibitory as well as excitatory local circuit elements, activation of VIPs and SOMs was consistent with the PC->SOM and PC->VIP synaptic dynamics shown in Figure 2A.

Several recent studies have identified VIPs as recipients of long-range excitatory input (Fu et al., 2014, Lee et al., 2013, Zhang et al., 2014). However, it is unclear to what extent local PCs innervate VIPs. To address this, we assessed the extent to which VIPs, compared to SOMs, are innervated by nearby PCs, by tracing presynaptic neurons of VIPs and SOMs with rabies (see Methods). Since similar experiments have been performed in V1 (Fu et al., 2014, Zhang et al., 2014), we did this in S1. This yielded tissue sections where SOM or VIP starter cells carry both nucleus-localized GFP and cytoplasmic mCherry, and cells presynaptic to these express only mCherry (Figure 2C). Most presynaptic cells (68%, 8643/12641 cells) had clear pyramidal morphology (Figure 2D), while 13% (1594/12641) were not pyramidal, i.e. likely INs with small, round bipolar or multipolar somata, and 19% (2404/12641) we were unable to reliably categorize based on soma morphology. These proportions were not significantly different between VIP-cre (PCs 65 ± 4 %, INs 11 ± 2 %, ambiguous 23 ± 3 %) and SOM-cre brains (PCs 70 ± 6 %, INs 13 ± 2 %, ambiguous 18 ± 4 %, $P > 0.27$ for each comparison). This is consistent with the much higher proportion of PCs than INs in cortex. We counted starter and presynaptic cells at the injection site across 4 VIP-cre and 3 SOM-cre brains and found that VIPs and SOMs get input from nearby cells to a similar extent (Figure 2E, VIPs: 93 ± 29 starters and 1259 ± 409 presynaptic cells/brain; SOMs: 118 ± 14 starters and 2535 ± 641 presynaptic cells/brain; $P > 0.1$). We annotated positions of labelled somata in the coronal sections and aligned these maps by the pial surface. The resulting average cell density heat maps (Figure 2F, S2A,B) indicate that both cell types receive input most heavily from L2/3. The layer differences in VIP and SOM starters were characteristic of their layer-distribution (Figure S2C). These data show that, in addition to the long-range inputs described previously, VIPs get excitatory synaptic input from nearby PCs to a similar extent as SOMs. This local excitation may thus be the most important driver of interneurons (Hofer et al., 2011, Kerlin et al., 2010).

VIPs and SOMs are excited by non-overlapping sets of nearby excitatory cells

To assess differences in spontaneous excitatory input to VIPs and SOMs in the same preparation, we made simultaneous current clamp recordings from them in slices from VIP-

cre: :LSL-TOM: :SOM-GFP(GIN) animals. When recording from two VIPs and two SOMs simultaneously in current clamp, we sometimes observed spontaneous activations occurring simultaneously only in the SOMs, while the VIPs were instead hyperpolarized (Figure 3A). We quantified the occurrence of these events (defined as spontaneous depolarizing events exceeding 5 mV for at least 500 ms) and classified these as shared between two cells if they overlapped. The analyzed neuron pairs were recorded for 285–1700 s (n = 36 recorded pairs; 12 from S1 and 24 from V1) and average event frequency per neuron was 0.0031 ± 0.0006 Hz (n = 26 cells). Out of 62 SOM activations recorded with another SOM, 55 % were shared; while out of 91 SOM or VIP activations (all recordings contained one SOM and one VIP) only 8.8 % were shared; and out of 25 VIP activations recorded with another VIP, 24 % were shared (Figure 3B). Shared VIP activations were rare probably since VIPs had an overall lower frequency of spontaneous activations (VIPs 0.0017 ± 0.0008 Hz, SOMs 0.0044 ± 0.0009 Hz). These data hint at a SOM specific excitatory presynaptic population.

To get more fine-grained information about population specific excitation we also analyzed shared voltage fluctuations in the resting membrane potential of simultaneously recorded SOMs and VIPs. We generated subthreshold membrane potential cross-correlograms for all cell pairs within and between interneuron classes recorded in slices from triple transgenic mice (VIP-cre: :LSL-TOM: :SOM-GFP(GIN), VIP-cre: :LSL-TOM: :PV-GFP(G42) and PV-cre: :LSL-TOM: :SOM-GFP(GIN), see Methods; Figure 3C, S3A–C). All zero-offset correlation coefficients approached 0 at intersomatic distances above 150 mm (Fig 3D), suggesting that the correlation reflects shared synaptic inputs from nearby cells. We therefore used only neuron pairs closer than 150 μm for the following analyses (mean distances noted below). Correlation coefficients were not significantly different ($P > 0.4$) between SOM-SOM (0.054 ± 0.012, n = 13, intersomatic distance 57.4 ± 10.7 μm), VIP-PV (0.053 ± 0.016, n = 5, distance 56.9 ± 17.4 μm) and VIP-VIP pairs (0.041 ± 0.013, n = 11, distance 61.6 ± 11.9 μm). However VIP-SOM pairs had significantly lower correlations than all other pairs (0.014 ± 0.006, n = 18, $P < 0.05$, distance 61.8 ± 10.1 μm), supporting the notion that VIPs and SOMs are innervated by distinct sets of PCs. For comparison, we also measured cross-correlograms for PV-PV and PV-SOM pairs (Figure S3B,C). While PV-PV pairs had high zero-offset correlation coefficients (0.079 ± 0.029, n = 5), PV-SOM pairs had significantly lower correlations (0.016 ± 0.006, n = 18, P = 0.003, Figure S3C). In summary, membrane potential cross-correlations were high *within* populations and lowest *across* populations, with the exception of VIP-PV pairs.

To directly assay common presynaptic partners of VIPs and SOMs, we used 2-photon mapping (Yoshimura and Callaway, 2005) of the CaMKIIα-C1V1(E162T)-p2A-EYFP expressing VIP-cre: :LSL-TOM: :SOM-GFP(GIN) slices shown in Figure 2B. We recorded from a VIP and a SOM in voltage clamp at −70 mV while sequentially stimulating small, soma-sized volumes of the tissue with a 1040 nm 2-photon laser (Packer et al., 2012)(Figure 3E, see Methods). During these focal stimuli we observed excitatory post synaptic currents (EPSCs) which were rarely time-locked in both cells (Figure 3F). We counted EPSCs during the 130 ms following stimulation onset as ‘shared’ if they occurred in both cells within 4 ms, and as ‘not shared’ otherwise. To account for the baseline rate of spontaneous EPSCs, we also counted ‘shared’ and ‘not shared’ EPSCs during the 130 ms before each stimulus. For each neuron pair, total ‘not shared’ EPSC frequency increased from 18.7 ± 7.9 Hz before

stimulus to 19.6 ± 7.9 Hz following stimulus (n = 6 cell pairs, paired T-test P = 0.008) indicating that the stimulation reliably recruited presynaptic excitatory neurons. However there was no significant change in shared EPSCs from before (0.34 ± 0.15 Hz) to after stimulation (0.35 ± 0.16 Hz, paired T-test P = 0.74). Within the categories 'shared' and 'not shared', we subtracted the spontaneous EPSC counts before stimuli from those following it to obtain a metric we call laser-EPSCs (L-EPSCs, Figure 3G). Across experiments counts of 'not shared' L-EPSCs were significantly above zero (80.3 ± 34.9, z-test against zero, P = 0.02) while 'shared' L-EPSCs were not (−1.2 ± 9.5, z-test against zero, P = 0.90). Since these data suggest that VIPs and SOMs do not share presynaptic partners, as a positive control we ran the same protocol on PVs. We chose PVs because they had the highest subthreshold cross-correlations in our data (Figure S3C), suggesting that they share many presynaptic partners (Hofer et al., 2011). We used PV-cre: :LSL-TOM mice that were injected with AAV5-CaMKIIα-C1V1(E162T)-p2A-EYFP (Figure S3B). PV-PV pairs (n = 5) had 201 ± 96.0 'not shared' L-EPSCs (z-test against zero, P = 0.036) and 36.4 ± 8.6 'shared' L-EPSCs (z-test against zero, P = 0.00002) indicating that both common and unique inputs were recruited by the laser stimulation (Figure S3E–H). The proportion of 'shared' L-EPSCs from all L-EPSCs can be interpreted as an approximation of the percentage of shared presynaptic cells between the two recorded neurons (Yoshimura and Callaway, 2005). This proportion was 22.6 ± 5.6 % for PV-PV pairs and −0.8 ± 4.9 % for VIP-SOM pairs (P = 0.015, Figure 3H). The latter was not significantly different from zero (z-test against zero, P = 0.95) implying that VIPs and SOMs do not share presynaptic cells. Intersomatic distances between the recorded SOM-VIP (74 ± 19 μm, n = 6) and PV-PV pairs (50 ± 9 μm, n = 5) were not significantly different (P = 0.31). In aggregate, the data in Figures 3 and S3 suggest that SOMs and VIPs are innervated at least in part by non-overlapping excitatory subnetworks.

Synaptic connectivity among interneurons

The above data suggest that population specific local excitation is a driving mechanism for co-activity in VIP and SOM populations. We next asked how are synaptic connections between interneuron classes arranged to allow for population co-activity. To get connectivity and synaptic parameters of unitary connections, we recorded from SOMs, VIPs and PVs in slices from cell-type specific triple-transgenic animals (VIP-cre: :LSL-TOM: :SOM-GFP(GIN), VIP-cre: :LSL-TOM: :PV-GFP(G42) and PV-cre: :LSL-TOM: :SOM-GFP(GIN); see Methods; Figure 4A). Since the high reliability of cell-type specific labelling in the mouse lines used for cross-breeding has been documented before (Chattopadhyaya et al., 2004, Ma et al., 2006, Oliva et al., 2000, Pfeffer et al., 2013, Sippy and Yuste, 2013, Taniguchi et al., 2011), we only confirmed labelling in VIP-cre: :LSL-TOM with immunohistochemistry (86.3% of TOM cells were VIP-immunoreactive, while 94.9% of VIP-immunoreactive cells contained TOM). We recorded with whole cell patch clamp from up to four cells (spaced within 10–300 μm) simultaneously in L2/3 in coronal slices from V1 and S1.

The overall pattern of synaptic connectivity between INs was similar in V1 and S1 (Figure S4) and therefore we pooled these data in Figure 4 (n = 1009 trial connections in total). All connections between INs were inhibitory and hyperpolarizing at resting membrane

potentials indicated in Figure S5. SOMs and VIPs formed inhibitory connections in both directions frequently, with slightly lower probability in V1 than S1 (Figure S4). The only population with high probability of within-population inhibition was PVs. The lowest inhibitory connectivity rates were within SOMs (0%, in agreement with Hu et al., 2011, Ma et al., 2012), within VIPs and from VIPs to PVs (Figure S4). In contrast to previous findings (Pfeffer et al., 2013), we find that PVs inhibit IN targets unselectively (Figure 4A, S4). As outlined in recent literature (Lee et al., 2013, Pfeffer et al., 2013, Pi et al., 2013), VIPs are specialized to inhibit SOMs. Since it is possible that these connectivity profiles define subclasses within marker-defined IN populations (Rudy et al., 2011) we analyzed passive and active electrophysiological parameters within each connectivity category to look for consistent differences (Figure S5). However, there were no significant differences between connectivity categories within a marker defined population, suggesting that connectivity and electrophysiological subclasses do not correlate.

To study dynamics and summation of inhibitory postsynaptic potentials (IPSPs) we used 50 Hz AP trains, which correspond to instantaneous firing rates during AP bursts in vivo (Gentet et al., 2012, Polack et al., 2013) and are commonly used to study synaptic dynamics (Kapfer et al., 2007, Silberberg and Markram, 2007). Our recordings show that connections between VIPs and SOMs have particularly strong facilitating dynamics (Figure 4B–G). According to maximal IPSP amplitudes during the 50 Hz AP train (Figure 4C), connections between SOMs and VIPs tended to be the largest among all synapses tested, peaking at 2.4 ± 0.4 mV (SOM->VIP, n = 7) and 3.2 ± 0.7 mV (VIP->SOM, n = 7) hyperpolarization. We also drove synapses with 100 Hz pulse trains to probe the upper limit of their range (Gentet et al., 2012), and got similar results (Figure 4C). To compare IPSP summation in different connection categories, we computed a ‘summation ratio’ for each synaptic connection, by dividing the 50 Hz peak amplitude by the first IPSP amplitude. This metric describes the growth of the postsynaptic response during sustained input. Summation ratios were significantly higher in both SOM->VIP and VIP->SOM connections compared to others, with no other significant differences in the dataset (Figure 4D). Related to this high summation, the kinetics of IPSCs between SOMs and VIPs were slower than those from PVs to VIPs and PVs (Figure 4H–I). The rise times for PV->PV and PV->VIP connections were not significantly different ($P = 0.53$) while rise times increased with significant steps ($P < 0.05$) in the order PV->VIP, SOM->VIP, VIP->SOM (Figure 4I). Decay time constants for SOM->VIP were not significantly different from PV->VIP ($P = 0.47$) but increased with significant steps ($P < 0.005$) in the order PV->PV, SOM->VIP, VIP->SOM (Figure 4I). These data suggest that inhibitory synapses between SOMs and VIPs are the most facilitating potentially due to differences in the GABA receptor composition of these synapses and/or dendritic filtering of the synaptic potentials. Facilitating synapses are ideal for promoting activity of population members on >100 ms timescales through inhibition of a reciprocally connected inhibitory population (see next section).

We observed electrical coupling, seen as depolarizing and nearly instantaneous postsynaptic potentials (Figure 4J) in a subset of recordings. Electrical coupling was only seen within VIP, SOM or PV populations, in agreement with previous findings from populations excluding neurogliaform cells (Galarreta and Hestrin, 1999, Gibson et al., 1999, Simon et al., 2005). Between VIPs, the latency from presynaptic action potential onset to electrical

PSP onset was 0.28 ± 0.05 ms, while the chemical synaptic potentials among VIPs were hyperpolarizing and had longer latencies of 3.2 ± 0.3 ms, n = 8. Electrical coupling between SOMs had the highest occurrence in our dataset (Figure 4K,L) while within PVs we saw less electrical coupling than has been reported by others (Galarreta and Hestrin, 1999, Gibson et al., 1999) likely due to the sparse labelling of PVs in the PV-GFP(G42) line (Chattopadhyaya et al., 2004).

Taken together, the data in Figures 4 and S4 indicate that the co-activity of IN populations is underscored by a pattern of chemical and electrical synaptic connections that inhibit across populations, and disinhibit and excite population members. In addition, the data show that the inhibitory synapses between SOMs and VIPs are highly facilitating likely due to their slow kinetics.

Cooperativity of VIP and SOM populations in brain slices

Through the inhibitory synapses between VIPs and SOMs, these INs can disinhibit members of the same population, effectively increasing the co-activity of the population. To directly test the importance of this mechanism, we studied within-population cooperativity in an experimental paradigm that emphasizes the within-population disinhibition. Since the connectivity patterns (Figure S4) were similar in S1 and V1, we did the following experiments in both areas (Fig 5, Fig S1 and V1 data denoted in figure legends). We patched four SOMs and induced one, two or three population members to fire a 3 s, 50 Hz AP train while recording spontaneous firing from the fourth member of the same population (Figure 5A). Each recording consisted of 9–21 trials with 20 s intervals, and spontaneous firing rates during 3 s windows before, during and after the train were averaged across trials. To increase spontaneous firing rates, we did these experiments in a modified high-K ACSF (see Methods). As we increased the number of firing cells, the recorded cells fired more spontaneous APs during the train (Figure 5B,C). Driving three SOM cells to fire was sufficient to significantly increase firing in the fourth SOM (68 ± 22 % increase in spontaneous firing, n = 13, Figure 5B), demonstrating within-population recruitment. When sorted into the categories ‘increased firing’, ‘decreased firing’ and ‘no change’ (see Methods), the proportion of SOMs that increased firing grew with the number of cells induced to fire (Figure 5C).

To see if the inhibitory connections across populations (Figure 4) are important for this cooperativity, we blocked GABA-A and GABA-B receptors with 1 μM gabazine and 40 μM CGP35348 respectively (both receptors were blocked at once since the synaptic kinetics, Figure 4H–I, suggest presence of both receptors and there may be spill-over of GABA during this assay). In this dataset the firing rate of the recorded SOMs increased 58 ± 16 % when the other 3 SOMs were induced to fire in control conditions (while baseline firing rates were similar in control, 1.9 ± 0.2 Hz and during GABA receptor blockade, 1.9 ± 0.3 Hz, P = 0.68). This increase was significantly reduced to 16 ± 7 % during GABA receptor blockade (n = 7, paired t-test P = 0.007, Figure 5D,E), indicating that disinhibition of SOMs by SOMs is an important mechanism for their cooperative recruitment. The 16 ± 7 % firing rate increase during GABA receptor blockade was still significantly different from both before and after the train (paired t-test P < 0.05), suggesting that another mechanism, likely

electrical coupling between SOMs (Figure 4K,L), also contributes to the cooperativity. The role of electrical coupling was further suggested by higher firing rate increases in SOMs that were electrically coupled to one of the other 3 SOMs than in those that were not (Figure 5E).

As shown in Figure 5F, VIPs also increased firing rates when other nearby VIPs were induced to fire at 50 Hz (Figure 5F,G). This was evident as a significantly increased spontaneous firing rate during induced firing of three cells, but not during firing of one or two (Figure 5G). In contrast to SOMs, the VIPs had a larger 'decreased firing' class during firing of one cell (SOMs 5/20, Figure 5G, and VIPs 9/20, Figure 5C), which persisted in diminished proportions during firing of two and three cells (Figure 5H). This dissociation is in line with the marginal fraction of VIP->VIP inhibition and the complete lack of SOM->SOM inhibition (Figure S4). However, the 'increased firing' class grew in numbers with more VIPs firing (Figure 5H), indicating cooperative recruitment in this population as well.

Pharmacological blockade of GABA receptors like in Figure 5D–E, did not yield consistent results for VIP cooperativity (Figure 5I). This is likely due to the mixture of VIP->VIP interactions: disinhibition through SOMs, direct inhibition, and direct excitation through electrical coupling (Figure 4, S4), which are not expected to affect every VIP in equal proportion. As this variation could be characteristic of putative subclasses of VIP cells (Rudy et al., 2011), we inspected the active and passive electrophysiological properties of VIPs categorized by their cooperativity in control conditions or their change in cooperativity in response to GABA receptor blockers (Figure S5). However, there were no significant differences, suggesting that putative electrophysiologically defined VIP subclasses do not correlate with VIPs defined by their cooperativity properties. Since VIPs produce acetyl choline (ACh, von Engelhardt et al., 2007) and are also uniquely sensitive to it (Figure S6), we investigated its role in cooperativity by blocking nicotinic ACh receptors with mecamylamine (10 μM). In contrast to GABAergic blockade, this cholinergic blockade significantly reduced the firing rate increase (Figure 5I) suggesting that ACh released from VIPs helps recruit other VIPs during sustained activity. As the choline acetyl transferase containing cells in neocortex have highest overlap with VIP and calretinin (von Engelhardt et al., 2007), it is likely that only those VIPs with calretinin (~50% of VIPs) release ACh. The baseline firing rates were similar across pharmacological manipulations in VIPs (control 1.3 ± 0.2 Hz, GABA blockade 1.2 ± 0.2 Hz; control 1.3 ± 0.2 Hz, mecamylamine 1.3 ± 0.2 Hz, $P > 0.6$) indicating that saturation effects due to altered baselines are unlikely to account for the results. Like SOMs, VIPs also showed higher cooperativity when the recorded cell was electrically coupled to one of the other 3 VIPs (Figure 5I). Collectively, the results in Figure 5 are consistent with a role for reciprocal inhibition between populations (Figure 4, Figure 5J,K) and within-population excitation in facilitating within-population co-activity.

Discussion

Here we showed that SOMs and VIPs demonstrate within-population co-activity (Figure 1,5) on a timescale of hundreds of milliseconds, and previous work has shown that PVs act similarly (Hofer et al., 2011). Our data suggest that VIPs and SOMs recruit their population members through four mechanisms: electrical coupling, complete lack (SOMs) or relative scarcity (VIPs) of within-population inhibition (see also (Hu et al., 2011, Ma et al., 2012)),

strong within-population disinhibition through inhibition of the reciprocally inhibitory population, and self-excitation of VIPs via ACh release. Additionally, the surrounding excitatory network drives population co-activity with population-specific dynamics of excitation (Figure 2) and possibly through population-specific presynaptic PCs (Figure 3). We note however that as suitable loss-of-function experiments to test the contribution of these mechanisms to IN population co-activity do not yet exist (synaptic blockers simultaneously specific to both pre- and postsynaptic populations would be necessary), our data mostly imply the involvement of these mechanisms by correlation rather than directly. A key exception to this is shown in Figure 5D–E, which directly demonstrates the role of GABAergic inhibition in cooperative recruitment of SOMs. The recruitment of VIPs by exogenous ACh (Figure S6) and their mecamylamine-sensitive population-recruitment (Figure 5H), combined with their ability to produce ACh (von Engelhardt et al., 2007) suggest that ambient ACh recruits a positive feedback loop via VIPs.

While the IN populations can be conveniently categorized by the non-overlapping markers SOM, PV and VIP to utilize transgenic mice, we note that there are likely further subpopulations within these that should fit the cooperativity/co-activity framework described here on average for these broad populations. Although we did not find subdivisions that correlate with consistent differences in electrophysiological parameters (Figure S5), other metrics such as combinatorial marker expression may correlate with the connectivity and cooperativity categories shown here. We hypothesize for further studies that the INs within a nearby volume of cortex and within one of these populations (IN team “A”) might be co-active/cooperative while another team “B” of the same population further away might be completely independent of team A’s actions. This type of compartmentalization may help regulate cooperativity so that all population members across the neocortex do not co-activate after some threshold is passed.

The difference in VIP and SOM excitatory input dynamics (Figure 2A,B) indicates that if they receive local input simultaneously, they would not be driven to direct mutual inhibition through their similar inhibitory output onto each other (Figure 4). The situation is similar to motor coordination of agonist/antagonist muscle pairs where simultaneous contraction of both would not be energetically advantageous. Along this line of reasoning, it would make sense to segregate PC networks to feed only into one population of a mutually inhibitory pair of IN populations. Our data in Figures 3 and S3 support this hypothesis in the case of SOMs and VIPs. On the other hand, we found no evidence for bidirectional inhibition between PVs and VIPs (Figure 4, S4), and in line with this, no evidence for non-overlapping local drive based on their high membrane potential correlation (Figure 2). While we used naïve mice in our experiments, other evidence suggest that VIPs and PVs can wire into a mutually inhibitory dyad during learning (Donato et al., 2013, David et al., 2007), which might also necessitate rewiring them to different excitatory sources. The third pair of IN populations in our analysis, PVs and SOMs, are reciprocally inhibitory (Figure 4, S4) and receive local excitation with different dynamics (Beierlein et al., 2003, Reyes et al., 1998). They also had reduced membrane potential cross-correlations (Figure S2) suggesting non-overlapping local drive. In aggregate, these data suggest that non-overlapping excitatory input wiring might generalize for all reciprocally inhibitory IN population dyads. We should mention that PV co-activity (Hofer et al., 2011) was shown to arise from their shared

presynaptic excitatory cells (also shown here in Figure S3) and the high occurrence of electrical coupling within PVs (Galarreta and Hestrin, 1999, Gibson et al., 1999). Our data suggests that mutual inhibition between PVs and SOMs (Figure 4) also supports co-activity within both populations.

Taken together, these data suggest that PV, SOM and VIP populations achieve within-population co-activity through conserved network mechanisms, as if they are specialized to act as groups. IN population cooperativity may be advantageous to circuit operation by predictively amplifying the particular type of inhibition (dendrite targeting, perisomatic or disinhibitory) provided by the population. Thus these multiple cooperative specializations would operate together to deliver wider-spread and increased inhibition in a supralinear proportion to growing demand, for example when excitation is about to overwhelm the circuit and cause epilepsy. We therefore propose an updated standard model for IN connectivity in the neocortex featuring reciprocally inhibitory population dyads rather than sequential hierarchy of populations and groups rather than individual neurons as computational units (Figure 6).

Experimental Procedures

Animals

Animal handling and experimentation were carried out in accordance with the US National Institutes of Health and Columbia University Institutional Animal Care and Use Committee guidelines. See Supplemental Experimental Procedures strain and breeding details.

Virus injections

Three to four weeks prior to the experiments VIP-cre: :LSL-TOM and SOM-cre: :LSL-TOM mice were injected stereotactically with AAV1-syn-GCaMP6s (UNC vector core) for in vivo experiments (Figure 1), and VIP-cre: :LSL-TOM: :SOM-GFP(GIN) or PV-cre: :LSL-TOM mice were injected with AAV5-CaMKIIa-C1V1(E162T)-p2A-EYFP (UNC vector core) for slice experiments (Figure 2B, Figure 3E–H, Figure S3D–G). Injection surgery was performed as in (Packer et al., 2012, see Supplemental Experimental Procedures). Rabies tracing was performed similarly to (Fu et al., 2014): VIP and SOM cells in S1 were labelled in VIP-cre: :LSL-tTA and SOM-cre: :LSL-tTA mice respectively with a tTA dependent helper virus (AAV2/9-TRE-hGFP-TVA-G, produced by the UNC vector core). Three weeks later the same injection site was infected with a pseudotyped rabies virus carrying mCherry (EnvA-pseudotyped, protein G-deleted rabies-EnvA-SAD-ΔG-mCherry virus, produced by the Viral Vector Core Facility at Salk Institute). After one week for the rabies virus to pass retrogradely across one synapse and express mCherry, brains were collected for immunostaining and analysis (see Supplemental Experimental Procedures).

In vivo experiments

Two weeks after viral delivery mice were anaesthetized with isoflurane, the scalp infiltrated with lidocaine and a custom-made titanium head plate was attached to the skull using dental cement. A 2 × 2 mm area of skull above the left V1 was partially thinned with a drill and covered with a silicone polymer. The mice received single doses of anti-inflammatory drugs

(0.6mg/kg dexamethasone and 5mg/kg enrofloxacin) as well as 5mg/kg carprofen injections for three days as post-operative pain medication and over the following week were briefly trained for head-fixed awake experiments in 2–3 sessions of increasing length on the experimental running-wheel apparatus.

On the day of the experiment P60–120 mice were anaesthetized with isoflurane and the skull was thinned to < 100 μm. The animal recovered from this brief (< 0.5 h) surgery for 1 h and was then imaged in a dark room for 2–3 h head-fixed on a running disk allowing the animal to move or remain stationary ad libitum. Throughout imaging sessions, we recorded the movement of the running disk via a custom-built infra-red optical mouse apparatus to distinguish between movement and stationary epochs as this is known to modulate V1 neurons (Fu et al., 2014, Polack et al., 2013, Reimer et al., 2014, Vinck et al., 2015).

Two-Photon Ca^{+2} Imaging

Changes in GCaMP6s fluorescence were imaged with a Two-photon Moveable Objective Microscope (Sutter) and a mode-locked Ti:sapphire laser (Chameleon Vision II, Coherent) at 950 nm through a 25 x (1.05 NA, Olympus) water immersion objective at 4.07 fps with 512 × 512 pixels resolution using Mscan software (Sutter). Images were obtained with a 535/50 and 610/75 nm band-pass emission filters for the green and red channels, respectively. Each field-of-view (FOV) contained 4–19 Ca2+ indicator filled VIPs or SOMs. Imaging data was analyzed using ImageJ and custom routines in MATLAB (see Supplemental Experimental Procedures).

Slice electrophysiology

Coronal brain slices from P21–180 animals were prepared according to standard methods (see Supplemental Experimental Procedures). Patch clamp recordings were performed in a submerged chamber in either standard artificial cerebrospinal fluid (ACSF) or a modified high K-ACSF (Figure 3A–D, Figure 5, see Supplemental Experimental Procedures). 4–8 MOhm patch pipettes were filled either with a K-gluconate (for current clamp) or Cs-methylsulphonate (for voltage clamp) based intracellular solution (see Supplemental Experimental Procedures). Gabazine (SR-95531) hydrobromide, CGP 35348 and mecamylamine hydrochloride were bought from Tocris and dissolved in ACSF. Whole cell recordings were not analysed if the access resistance was above 25 MOhm. Most recordings were performed at 24 °C for increased stability. Datasets in Figure 5 and Figure 2A,B contain recordings at 35–37 °C (which were not different from recordings at 24 °C), performed to ensure that temperature effects do not confound our main conclusions. In Figure 5, when necessary, cells were injected sustained current of < 50 pA to maintain average firing rates between 1 – 10 spikes/3 s (average during 3 s before induced firing was 4.6 ± 0.3 spikes/3 s). In the GABAergic blockade experiments for Figure 5, ~70% of recordings developed epileptiform activity seen as global 0.5–1 s bursts occurring at a mean frequency of 0.1–0.001 Hz. Trials containing these bursts in the analysis windows were removed from analysis. In Figure 3C,D and S3A–C the recorded cells were injected up to 100 pA current to keep their firing to a minimum. The amount of injected current was not changed during recordings in Figs 3A–D, 5 or S3A–C. See Supplemental Experimental Protocols for photo-stimulation protocols used in Figures 2B, 3E–H and S3E–G.

Electrophysiology analysis

Most patch clamp data were analyzed with custom routines in Matlab. In Figure 5C and G, we categorized the response of a recorded cell by two separate comparisons: the firing rate during the induced firing train compared to 1) before and 2) after it in the firing rate histogram averaged across 9–21 trials. Recorded cells were categorized as 'increased firing' if there were more APs during the train compared to the three seconds both before and after the train, 'decreased firing' if there were less APs during the train compared to both before and after the train, and 'no change' if the difference between firing during the train compared to before had opposite sign of firing during the train compared to after. EPSCs in Figures 3E–H and S3E–G were detected semi-manually in Minianalysis (Synaptosoft). Cross-correlation data in Figure 3C,D and S3A–C were obtained from continuous current clamp traces lasting 285–1860 s by first deleting from all simultaneously recorded traces, epochs with action potentials along with the 10 ms before and 100 ms after the times when any trace crossed 0 mV. This procedure eliminated < 5 s from each trace. After this the traces were high-pass filtered above 0.0005 Hz to remove slow components due to electrode potential drift that can bias the analysis, and then cross-correlograms were generated.

Statistics

All data are shown as mean ± SEM unless stated otherwise. Statistical significance was determined by unpaired Student t-tests unless stated otherwise. All statistics were performed using statistical functions in Matlab or Excel.

Supplementary Material

Refer to Web version on PubMed Central for supplementary material.

Acknowledgments

The project was supported by NEI (DP1EY024503, R01EY011787), NIMH (R01MH101218, R01 MH100561), DARPA SIMPLEX N66001-15-C-4032 and U. S. Army Research Office under contract number W911NF-12-1-0594 MURI (to RY), HFSP LTF (to MMK), Canadian Institute for Health Research fellowship (to JJ) and Marie Curie IOF (to IA). We thank Darcy Peterka, Yeonsook Shin and Alexa Semonche for technical assistance and Denis Burdakov, Attila Gulyas, Michael Kohl, Ole Paulsen, Jochen Staiger, Jae-eun Miller and Luis Carillo-Reid for advice and critical reading of the manuscript, as well as Josh Z Huang for providing facilities and resources.

References

Bathellier B, Ushakova L, Rumpel S. Discrete neocortical dynamics predict behavioral categorization of sounds. Neuron. 2012; 76:435–449. [PubMed: 23083744]

Beierlein M, Gibson JR, Connors BW. Two dynamically distinct inhibitory networks in layer 4 of the neocortex. Journal of neurophysiology. 2003; 90:2987–3000. [PubMed: 12815025]

Ch'ng YH, Reid RC. Cellular imaging of visual cortex reveals the spatial and functional organization of spontaneous activity. Frontiers in integrative neuroscience. 2010:4. [PubMed: 20300470]

Chattopadhyaya B, Di Cristo G, Higashiyama H, Knott GW, Kuhlman SJ, Welker E, Huang ZJ. Experience and activity-dependent maturation of perisomatic GABAergic innervation in primary visual cortex during a postnatal critical period. J Neurosci. 2004; 24:9598–9611. [PubMed: 15509747]

Cottam JC, Smith SL, Hausser M. Target-specific effects of somatostatin-expressing interneurons on neocortical visual processing. J Neurosci. 2013; 33:19567–1978. [PubMed: 24336721]

Coultrap SJ, Bayer KU. CaMKII regulation in information processing and storage. Trends Neurosci. 2012; 35:607–618. [PubMed: 22717267]

Cowansage KK, Shuman T, Dillingham BC, Chang A, Golshani P, Mayford M. Direct reactivation of a coherent neocortical memory of context. Neuron. 2014; 84:432–441. [PubMed: 25308330]

David C, Schleicher A, Zuschratter W, Staiger JF. The innervation of parvalbumin-containing interneurons by VIP-immunopositive interneurons in the primary somatosensory cortex of the adult rat. The European journal of neuroscience. 2007; 25:2329–2340. [PubMed: 17445231]

Donato F, Rompani SB, Caroni P. Parvalbumin-expressing basket-cell network plasticity induced by experience regulates adult learning. Nature. 2013; 504:272–276. [PubMed: 24336286]

Fu Y, Tucciarone JM, Espinosa JS, Sheng N, Darcy DP, Nicoll RA, Huang ZJ, Stryker MP. A cortical circuit for gain control by behavioral state. Cell. 2014; 156:1139–1152. [PubMed: 24630718]

Galarreta M, Hestrin S. A network of fast-spiking cells in the neocortex connected by electrical synapses. Nature. 1999; 402:72–75. [PubMed: 10573418]

Gentet LJ, Kremer Y, Taniguchi H, Huang ZJ, Staiger JF, Petersen CCH. Unique functional properties of somatostatin-expressing GABAergic neurons in mouse barrel cortex. Nature neuroscience. 2012; 15:607–612. [PubMed: 22366760]

Gibson JR, Beierlein M, Connors BW. Two networks of electrically coupled inhibitory neurons in neocortex. Nature. 1999; 402:75–79. [PubMed: 10573419]

Hangya B, Pi H-J, Kvitsiani D, Ranade SP, Kepecs A. From circuit motifs to computations: mapping the behavioral repertoire of cortical interneurons. Current opinion in neurobiology. 2014; 26:117–124. [PubMed: 24508565]

Harris KD. Neural signatures of cell assembly organization. Nature reviews Neuroscience. 2005; 6:399–407. [PubMed: 15861182]

Harris KD, Shepherd GMG. The neocortical circuit: themes and variations. Nature neuroscience. 2015; 18:170–181. [PubMed: 25622573]

Hebb, DO. The organization of behavior; a neuropsychological theory. New York: Wiley; 1949.

Hofer SB, Ko H, Pichler B, Vogelstein J, Ros H, Zeng H, Lein E, Lesica NA, Mrsic-Flogel TD. Differential connectivity and response dynamics of excitatory and inhibitory neurons in visual cortex. Nat Neurosci. 2011; 14:1045–1052. [PubMed: 21765421]

Hu H, Ma Y, Agmon A. Submillisecond firing synchrony between different subtypes of cortical interneurons connected chemically but not electrically. J Neurosci. 2011; 31:3351–3361. [PubMed: 21368047]

Ji D, Wilson MA. Coordinated memory replay in the visual cortex and hippocampus during sleep. Nat Neurosci. 2007; 10:100–107. [PubMed: 17173043]

Kapfer C, Glickfeld LL, Atallah BV, Scanziani M. Supralinear increase of recurrent inhibition during sparse activity in the somatosensory cortex. Nature neuroscience. 2007; 10:743–753. [PubMed: 17515899]

Kepecs A, Fishell G. Interneuron cell types are fit to function. Nature. 2014; 505:318–326. [PubMed: 24429630]

Kerlin AM, Andermann ML, Berezovskii VK, Reid RC. Broadly tuned response properties of diverse inhibitory neuron subtypes in mouse visual cortex. Neuron. 2010; 67:858–871. [PubMed: 20826316]

Lee S, Kruglikov I, Huang ZJ, Fishell G, Rudy B. A disinhibitory circuit mediates motor integration in the somatosensory cortex. Nat Neurosci. 2013; 16:1662–1670. [PubMed: 24097044]

Lee SH, Kwan AC, Zhang S, Phoumthipphavong V, Flannery JG, Masmanidis SC, Taniguchi H, Huang ZJ, Zhang F, Boyden ES, Deisseroth K, Dan Y. Activation of specific interneurons improves V1 feature selectivity and visual perception. Nature. 2012; 488:379–383. [PubMed: 22878719]

Luczak A, Bartho P, Harris KD. Spontaneous events outline the realm of possible sensory responses in neocortical populations. Neuron. 2009; 62:413–425. [PubMed: 19447096]

Ma Y, Hu H, Agmon A. Short-term plasticity of unitary inhibitory-to-inhibitory synapses depends on the presynaptic interneuron subtype. J Neurosci. 2012; 32:983–988. [PubMed: 22262896]

Ma Y, Hu H, Berrebi AS, Mathers PH, Agmon A. Distinct subtypes of somatostatin-containing neocortical interneurons revealed in transgenic mice. J Neurosci. 2006; 26:5069–5082. [PubMed: 16687498]

Miller J-EK, Ayzenshtat I, Carrillo-Reid L, Yuste R. Visual stimuli recruit intrinsically generated cortical ensembles. Proc Natl Acad Sci U S A. 2014; 111:E4053–E4061. [PubMed: 25201983]

Oliva AA Jr, Jiang M, Lam T, Smith KL, Swann JW. Novel hippocampal interneuronal subtypes identified using transgenic mice that express green fluorescent protein in GABAergic interneurons. J Neurosci. 2000; 20:3354–3368. [PubMed: 10777798]

Packer AM, Peterka DS, Hirtz JJ, Prakash R, Deisseroth K, Yuste R. Two-photon optogenetics of dendritic spines and neural circuits. Nat Methods. 2012; 9:1202–1205. [PubMed: 23142873]

Pfeffer CK, Xue M, He M, Huang ZJ, Scanziani M. Inhibition of inhibition in visual cortex: the logic of connections between molecularly distinct interneurons. Nat Neurosci. 2013; 16:1068–1076. [PubMed: 23817549]

Pi HJ, Hangya B, Kvitsiani D, Sanders JI, Huang ZJ, Kepecs A. Cortical interneurons that specialize in disinhibitory control. Nature. 2013; 503:521–524. [PubMed: 24097352]

Polack PO, Friedman J, Golshani P. Cellular mechanisms of brain state-dependent gain modulation in visual cortex. Nat Neurosci. 2013; 16:1331–1339. [PubMed: 23872595]

Reimer J, Froudarakis E, Cadwell CR, Yatsenko D, Denfield GH, Tolias AS. Pupil fluctuations track fast switching of cortical states during quiet wakefulness. Neuron. 2014; 84:355–362. [PubMed: 25374359]

Reyes A, Lujan R, Rozov A, Burnashev N, Somogyi P, Sakmann B. Target-cell-specific facilitation and depression in neocortical circuits. Nature neuroscience. 1998; 1:279–285. [PubMed: 10195160]

Root CM, Denny CA, Hen R, Axel R. The participation of cortical amygdala in innate, odour-driven behaviour. Nature. 2014; 515:269–273. [PubMed: 25383519]

Rudy B, Fishell G, Lee S, Hjerling-Leffler J. Three groups of interneurons account for nearly 100% of neocortical GABAergic neurons. Developmental neurobiology. 2011; 71:45–61. [PubMed: 21154909]

Runyan CA, Schummers J, Van Wart A, Kuhlman SJ, Wilson NR, Huang ZJ, Sur M. Response features of parvalbumin-expressing interneurons suggest precise roles for subtypes of inhibition in visual cortex. Neuron. 2010; 67:847–857. [PubMed: 20826315]

Sakata S, Harris KD. Laminar structure of spontaneous and sensory-evoked population activity in auditory cortex. Neuron. 2009; 64:404–418. [PubMed: 19914188]

Silberberg G, Markram H. Disynaptic inhibition between neocortical pyramidal cells mediated by Martinotti cells. Neuron. 2007; 53:735–746. [PubMed: 17329212]

Simon A, Olah S, Molnar G, Szabadics J, Tamas G. Gap-junctional coupling between neurogliaform cells and various interneuron types in the neocortex. J Neurosci. 2005; 25:6278–6285. [PubMed: 16000617]

Sippy T, Yuste R. Decorrelating action of inhibition in neocortical networks. J Neurosci. 2013; 33:9813–9830. [PubMed: 23739978]

Sohya K, Kameyama K, Yanagawa Y, Obata K, Tsumoto T. GABAergic neurons are less selective to stimulus orientation than excitatory neurons in layer II/III of visual cortex, as revealed by in vivo functional Ca2+ imaging in transgenic mice. J Neurosci. 2007; 27:2145–2149. [PubMed: 17314309]

Taniguchi H, He M, Wu P, Kim S, Paik R, Sugino K, Kvitsiani D, Fu Y, Lu J, Lin Y, Miyoshi G, Shima Y, Fishell G, Nelson SB, Huang ZJ. A resource of Cre driver lines for genetic targeting of GABAergic neurons in cerebral cortex. Neuron. 2011; 71:995–1013. [PubMed: 21943598]

Vinck M, Batista-Brito R, Knoblich U, Cardin JA. Arousal and Locomotion Make Distinct Contributions to Cortical Activity Patterns and Visual Encoding. Neuron. 2015; 86:740–754. [PubMed: 25892300]

Von Engelhardt J, Eliava M, Meyer AH, Rozov A, Monyer H. Functional characterization of intrinsic cholinergic interneurons in the cortex. J Neurosci. 2007; 27:5633–5642. [PubMed: 17522308]

Yoshimura Y, Callaway EM. Fine-scale specificity of cortical networks depends on inhibitory cell type and connectivity. Nat Neurosci. 2005; 8:1552–1559. [PubMed: 16222228]

Zhang S, Xu M, Kamigaki T, Hoang Do JP, Chang WC, Jenvay S, Miyamichi K, Luo L, Dan Y. Selective attention. Long-range and local circuits for top-down modulation of visual cortex processing. Science. 2014; 345:660–665. [PubMed: 25104383]

Highlights

- VIP and SOM expressing interneuron populations have within-population co-activity.
- VIP and SOM interneurons receive distinct local excitation from pyramidal cells.
- VIP and SOM populations inhibit each other and disinhibit and excite themselves.
- Firing of a few VIP or SOM interneurons can recruit firing in population members.

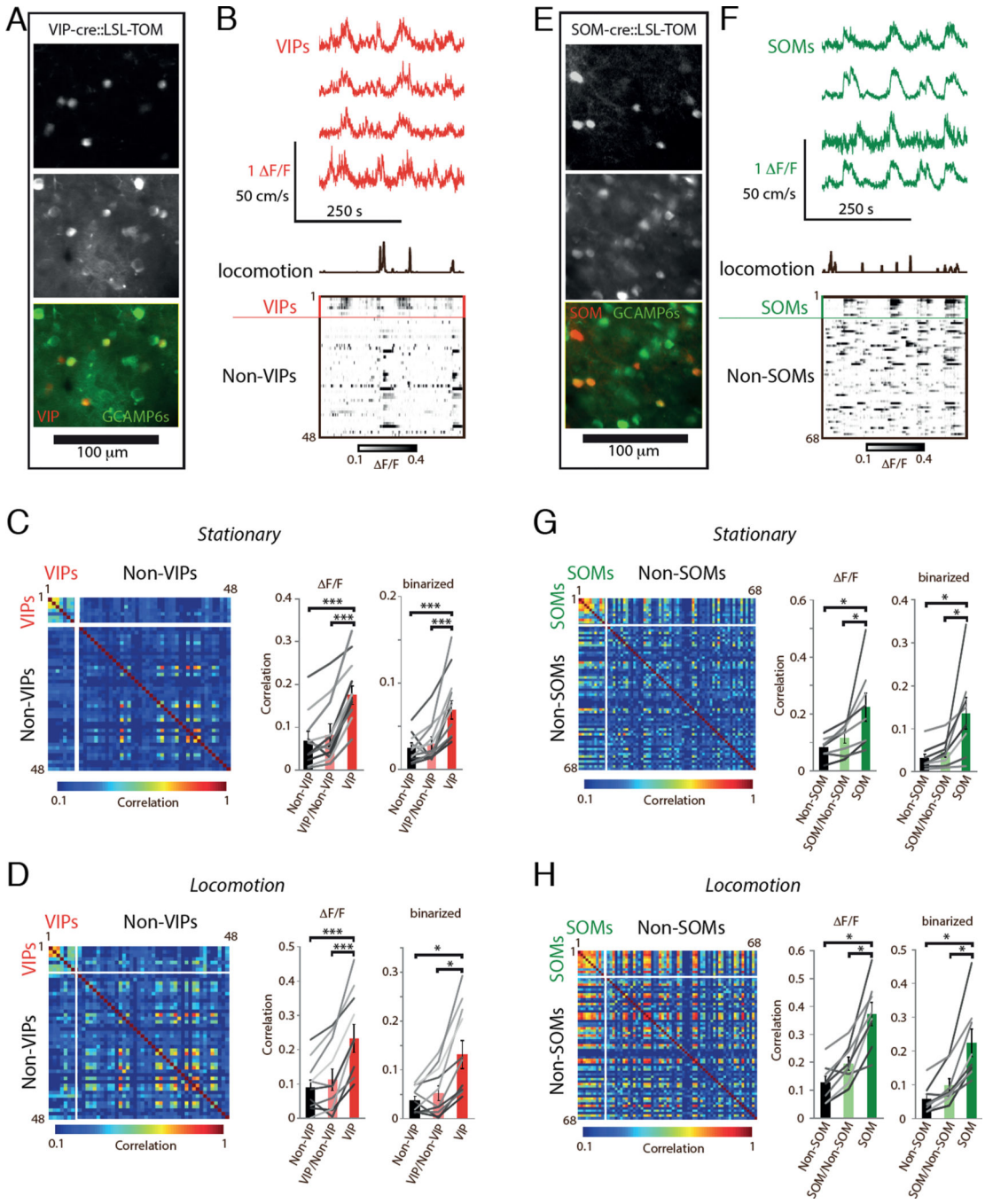

Figure 1. VIPs and SOMs tend to be active as populations in awake mice

(A) Standard deviation projection of Syn-GCaMP6s and average projection of VIP-TOM in V1 L2/3 of VIP-cre: :LSL-TOM.

(B) Example DF/F traces during ongoing activity. Red traces are from VIPs, black trace denotes when the mouse was running. Bottom DF/F raster is from VIP and non-VIP cells in the FOV as indicated.

(C) Calcium signal correlations when the mouse was stationary. Left, matrix of Pearson correlation coefficients for each cell pair in the data shown in B. Middle, ΔF/F correlation

coefficients for each pair averaged within categories (bars; Non-VIP, R = 0.07 ± 0.02; VIP/Non-VIP, R = 0.08 ± 0.03; VIP, R = 0.18 ± 0.02); gray lines connect values from each FOV. Right, same as middle, using binarized data (Non-VIP, R = 0.02 ± 0.01; VIP/Non-VIP, R = 0.03 ± 0.01; VIP, R = 0.07 ± 0.01).

(D) Calcium signal correlations during locomotion. Notation as in C (Middle, bars: Non-VIP, R = 0.09 ± 0.02; VIP/Non-VIP, R = 0.11 ± 0.03; VIP, R = 0.23 ± 0.04; Right, bars: Non-VIP, R = 0.04 ± 0.01; VIP/Non-VIP, R = 0.05 ± 0.01; VIP, R = 0.13 ± 0.03). Same movies as in C, except one that contained too few locomotion frames.

(E) Syn-GCaMP6s expression in V1 L2/3 of SOM-cre: :LSL-TOM mouse.

(F) Example DF/F traces during ongoing activity. Red traces are from VIPs, black trace denotes when the mouse was running. Bottom DF/F raster is from VIP and non-VIP cells in the FOV as indicated. All traces are aligned in time and in the same time scale.

(G) Calcium signal correlations when the mouse was stationary. Notation as in C (Middle, bars: Non-SOM, R = 0.08 ± 0.01; SOM/Non-SOM, R = 0.12 ± 0.02; SOM, R = 0.22 ± 0.05; right, bars: Non-SOM, R = 0.03 ± 0.01; SOM/Non-SOM, R = 0.04 ± 0.01; SOM, R = 0.13 ± 0.04).

(H) Calcium signal correlations during locomotion. Notation as in C (bars; Non-SOM, R = 0.13 ± 0.02; SOM/Non-SOM, R = 0.20 ± 0.02; SOM, R = 0.37 ± 0.04; right, bars: Non-SOM, R = 0.06 ± 0.01; SOM/Non-SOM, R = 0.10 ± 0.02; SOM, R = 0.22 ± 0.04). In panels C-H, *, $P < 0.05$; ***, $P < 0.0005$ by paired T-test.

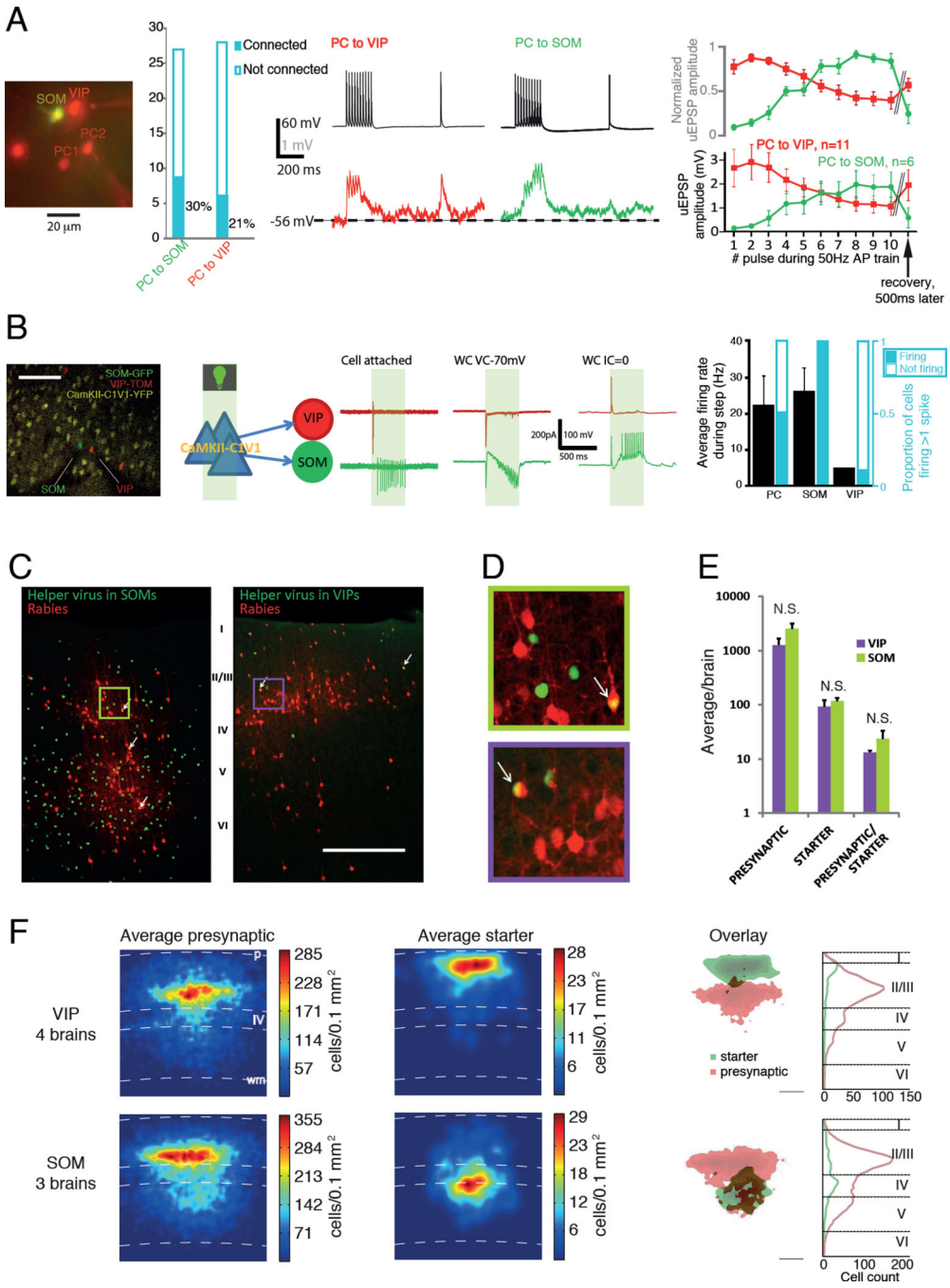

Figure 2. L2/3 PC innervation of VIPs and SOMs

(A) From left to right: a representative image taken while patching a SOM, a VIP and two PCs; connection probabilities PC->SOM and PC->VIP; example traces of PC->VIP and PC->SOM connections with traces from postsynaptic INs in color and presynaptic PC traces in black; dynamics of 50 Hz unitary excitatory post synaptic potential (uEPSP) trains onto VIPs (n = 11; 6 from S1 and 5 from V1) and SOMs (n = 6; all from V1) normalized to maximum amplitude (top) and as raw data (bottom).

(B) From left to right: representative image taken while patching a SOM and a VIP in a VIP-cre: :LSL-TOM: :SOM-GFP(GIN) slice expressing CaMKII-C1V1-YFP; schematic of experiment and cell attached, whole cell (WC) voltage clamp (VC) and current clamp (IC) traces of a VIP and SOM recorded simultaneously while exciting the tissue with green light (shaded 500 ms period); summary of PC, SOM and VIP firing during the light step after an initial spike at the beginning (all recordings from S1).

(C) Example confocal micrographs of coronal sections from rabies tracing of SOMs (left) and VIPs (right). Starter cells are labelled with arrows. Red cells are presynaptic to starters.

(D) Enlarged views from colored boxes in C showing typical pyramidal morphologies of presynaptic cells.

(E) Summary cell counts and presynaptic/starter ratios near the injection site from 4 VIP-cre and 3 SOM-cre brains.

(F) Left, heat maps averaged across coronal sections spanning the injection sites. Right, overlaid starter (in green) and presynaptic (in red) cell heat maps and layer distributions of cell counts. All scale bars are 200 μm, p = Pia, IV = Layer 4, wm = white matter boundary. See Figure S2 for separate data from each brain. Data in C-F and Figure S2 are from S1 cortex.

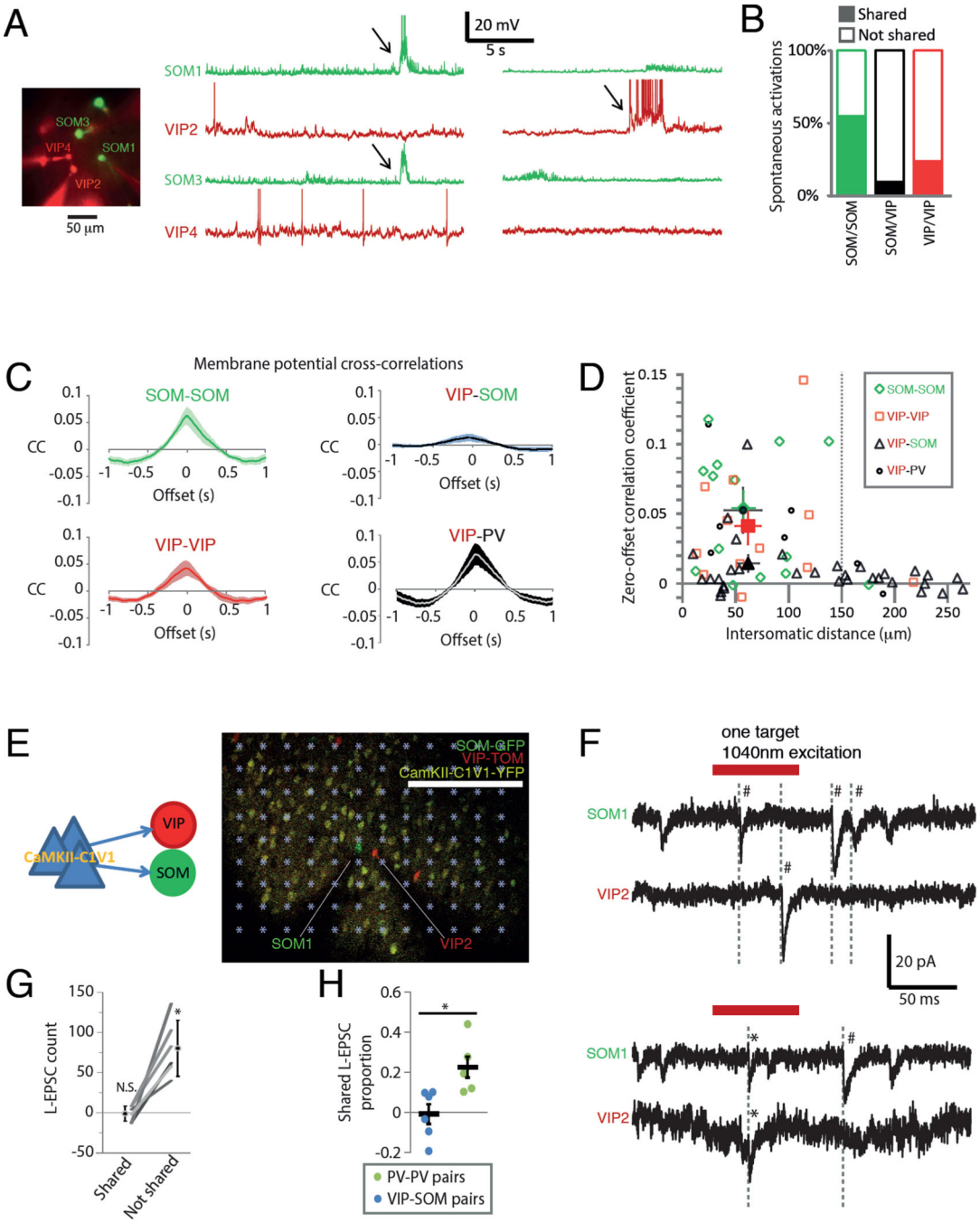

Figure 3. Distinct presynaptic excitatory cells innervate VIPs and SOMs

(A) Example whole cell current clamp recording of two SOMs and two VIPs simultaneously in a VIP-cre: :LSL-TOM: :SOM-GFP(GIN) slice showing spontaneous activation (denoted by arrows) of only the SOMs or one of the VIPs. Action potentials are truncated at −10 mV. (B) Summary of the occurrence of simultaneous (shared) activation of the indicated two cells. “Not shared” activations were those occurring in one cell only, while both cells were being recorded. Pooled data from S1 and V1 as indicated in text.

(C) Average subthreshold membrane potential cross-correlograms from cell pairs less than 150 mm apart (SOM-SOM 13 pairs, 4 in S1 and 9 in V1; VIP-SOM 18 pairs, 8 in S1 and 10 in V1; VIP-VIP 11 pairs, 3 in S1 and 8 in V1; VIP-PV 5 pairs, all in V1). See Figure S3 for all individual pair cross-correlograms.

(D) Correlation coefficients (at time lag 0s) for each recorded cell pair as a function of intersomatic distance. Mean ± sem for cell pairs of each category less than 150 mm apart plotted as larger symbols with error bars.

(E) Schematic of 2-photon input mapping experiment (left) and micrograph of a recording (right). Asterisks on top of the image represent stimulation targets.

(F) Representative voltage clamp (−70 mV) traces from a SOM and a VIP showing shared (*) and not shared (#) EPSCs.

(G) Shared and not shared L-EPSCs (see text) for 6 SOM-VIP pairs. Shared and not shared counts from the same experiment are connected by a line and mean ± sem are shown next to them. *, P = 0.02; N.S., P = 0.90 by z-test against zero.

(H) Proportion of shared L-EPSCs from individual experiments (circles) and mean ± sem (lines). N = 6 SOM-VIP pairs and 5 PV pairs (all from S1); *, P = 0.015.

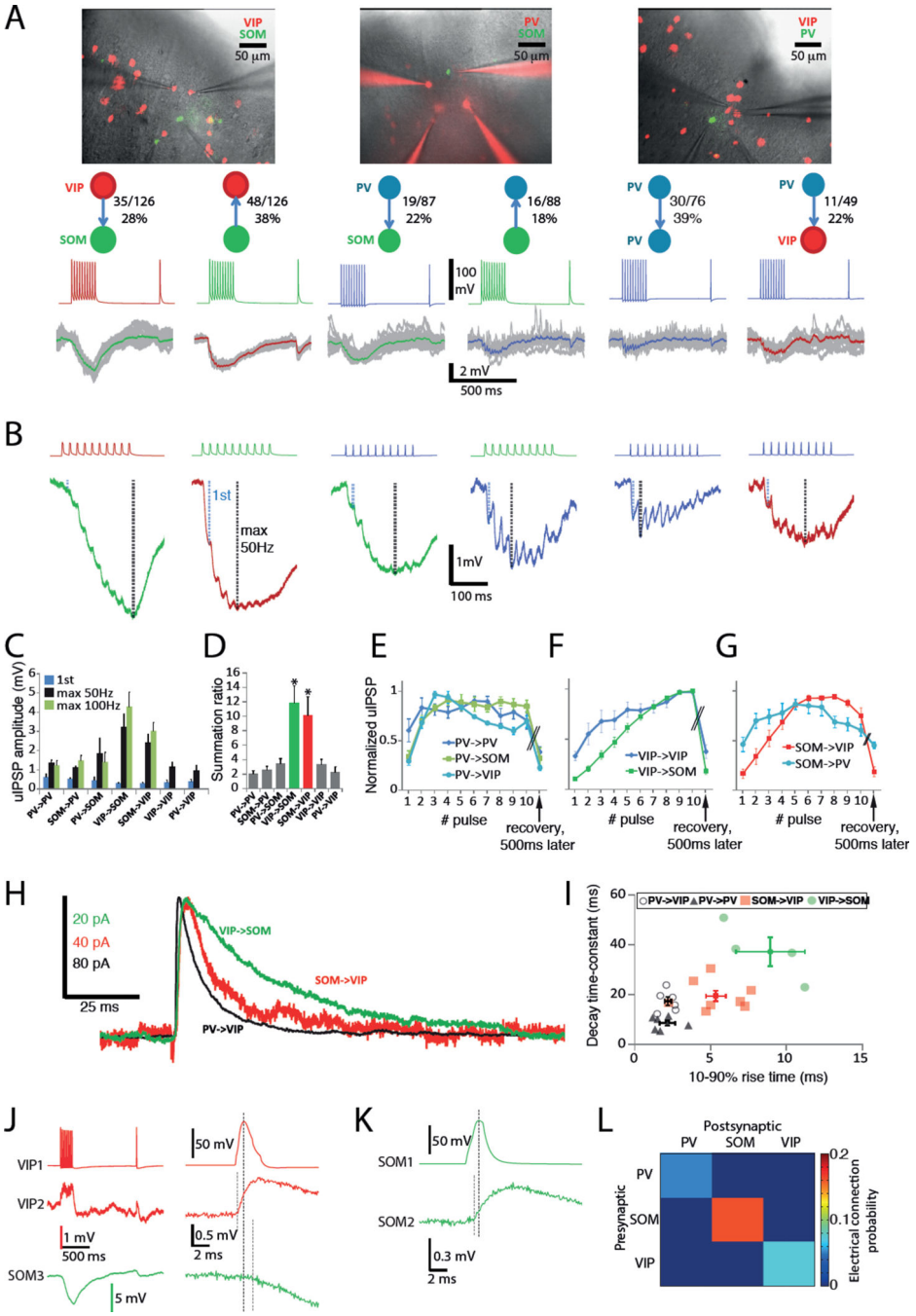

Figure 4. Chemical and electrical synaptic connectivity supports within-population co-activity

(A) Images and example recordings from triple transgenic slices. Overlaid gray traces are postsynaptic responses from 10–20 trials and colored trace on top is average. Combined connection probabilities from S1 and V1 are noted next to each main connection type (separated by area in Figure S4). Total number of trial connections is n = 1009.

(B) Enlarged postsynaptic traces from A showing key differences in dynamics and summation of each main connection category.

(C) Mean ± sem of amplitudes from combined data from S1 and V1 (n = 3–19 for each bar). Amplitudes of the first IPSP in a train were significantly smaller ($P < 0.01$) in both SOM->VIP (0.30 ± 0.04 mV, n = 19) and VIP->SOM (0.31 ± 0.04 mV, n = 18) than PV->PV (0.58 ± 0.10 mV, n = 13) and SOM->PV (0.53 ± 0.07 mV, n = 12). There were no other significant differences in first IPSP amplitudes (PV->SOM 0.45 ± 0.18 mV, n = 7; VIP->VIP 0.37 ± 0.11 mV, n = 5; PV->VIP 0.40 ± 0.10 mV, n = 3). PV->PV (1.2 ± 0.2 mV, n = 7) and SOM->PV (1.1 ± 0.1 mV, n = 7) were the only 50Hz peak amplitudes significantly smaller ($P < 0.05$) than both SOM->VIP (2.4 ± 0.4 mV, n = 7) and VIP->SOM (3.2 ± 0.7 mV, n = 7). Other 50Hz peak amplitudes: PV->SOM 1.9 ± 0.8 mV, n = 5; VIP->VIP 1.2 ± 0.3 mV, n = 5; PV-VIP 0.9 ± 0.3 mV, n = 3.

(D) Summation ratios (50 Hz peak amplitude / first IPSP amplitude, n = 3–19 for each bar) for each connection type. *, $P < 0.05$ compared to gray bars.

(E) – (G) Average ± sem uIPSP amplitudes normalized to maximum responses during a 50 Hz AP train for each category of connection (n = 3–19 for each curve).

(H) Example voltage clamp recordings (+40 mV holding potential) of unitary IPSCs.

(I) Scatter data (light symbols) and mean ± sem (symbols with error bars) of uIPSC rise and decay parameters. Rise times were PV->PV 2.2 ± 0.5 ms, n = 6; PV->VIP 2.2 ± 0.2 ms, n = 6; SOM->VIP 5.3 ± 0.7 ms, n = 8; VIP->SOM 8.9 ± 2.3 ms, n = 4. Decay time constants were SOM->VIP 19.3 ± 2.1 ms, n = 8; PV->VIP 17.2 ± 1.7 ms, n = 6; PV->PV 8.4 ± 1.0 ms, n = 6; VIP->SOM 37.1 ± 5.7 ms, n = 4.

(J) Example traces of electrical coupling between two VIPs and a simultaneous inhibitory connection from the VIP to a SOM. Right panel, focused into first PSPs of the recording to show time difference between action-potential peak to electrical v chemical PSP onset (marked by dashed lines).

(K) Example of a SOM->SOM electrical connection.

(L) Combined electrical connection probability matrix from S1 and V1 (numbers by region in Figure S4).

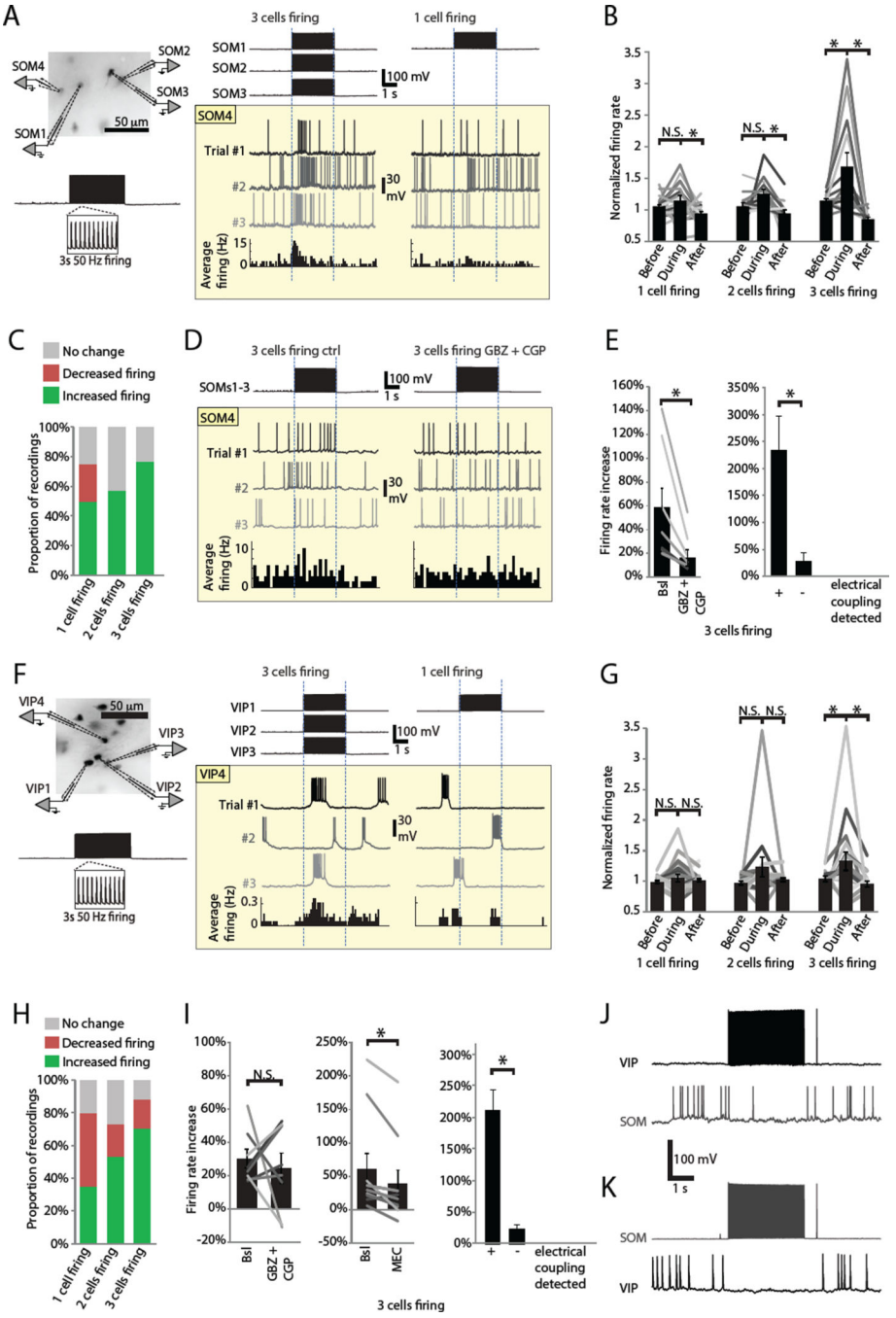

Figure 5. SOM and VIP functional cooperativity in brain slices

(A) Example recording of four SOMs that demonstrated higher cooperative recruitment during induced firing (50 Hz AP train for 3 s) of three cells than when only one cell was induced to fire. Three trials are shown for SOM4 in different shades of gray above a spike rate histogram across 15 trials.

(B) Normalized SOM firing rates (from recordings as in A). All individual recordings are shown as lines and the mean ± sem as bars *, $P < 0.05$; N.S., $P > 0.05$ by paired T-test.

Number of recordings in each category: ‘1 cell firing’ n = 20 (S1 n = 15; V1 n = 5), ‘2 cells firing’ n = 14 (S1 n = 6; V1 n = 8) and ‘3 cells firing’ n = 13 (S1 n = 7; V1 n = 6).

(C) Proportions of SOM recordings categorized (see Methods).

(D) Example recording where blockade of $GABA_A$ receptors with 1 mM gabazine and $GABA_B$ receptors with 40 μM CGP35348 attenuated the firing rate increase of the fourth SOM during firing of three SOMs.

(E) Left, Normalized firing rate changes from recordings as shown in D. All individual recordings are shown as lines, and mean ± sem as bars with error bars. *, P = 0.0065 by paired T-test; n = 7 (S1 n = 4; V1 n = 3). Right, normalized firing rate changes from recordings where the recorded SOM was electrically coupled to one of the others (+, n = 3), and those where the recorded SOM was not electrically coupled (−, n = 9; *, P = 0.027 by paired T-test).

(F) Example recording of four VIPs that demonstrated cooperative recruitment only during induced firing of three cells. Three trials are shown for VIP4 in different shades of gray above a spike rate histogram across 12 trials.

(G) Normalized VIP firing rates (from recordings as in G). Presented like B. *, P < 0.05; N.S., P > 0.05 by paired T-test. Number of recordings in each category: ‘1 cell firing’ n = 20 (S1 n = 5; V1 n = 15), ‘2 cells firing’ n = 16 (S1 n = 5; V1 n = 11) and ‘3 cells firing’ n = 18 (S1 n = 6; V1 n = 12).

(H) Proportions of VIP recordings categorized (see Methods).

(I) Left, blockade of GABA receptors as in D did not always attenuate firing rate increase of fourth VIP during firing of three VIPs; baseline firing rate increase 30 ± 6 %, in GABA blockers 24 ± 9 %, n = 8 (S1 n = 3; V1 n = 5). Center, blockade of ACh receptors with 10 mM mecamylamine (MEC) attenuated VIP cooperativity; baseline firing rate increase 61 ± 23 %, in MEC 39 ± 20 %, n = 10 (S1 n = 5; V1 n = 5). Presented like E. *, P = 0.007; N.S., P = 0.54 by paired T-test. Right, normalized firing rate changes from recordings where the recorded VIP was electrically coupled to one of the others (+, n = 4), and those where the recorded VIP was not electrically coupled (−, n = 16; *, $P < 10^{-7}$ by paired T-test).

(J) 3 s of 50 Hz firing in two VIPs simultaneously silences spontaneous firing of a nearby SOM.

(K) 3 s of 50 Hz firing in two SOMs simultaneously silences spontaneous firing of a nearby VIP.

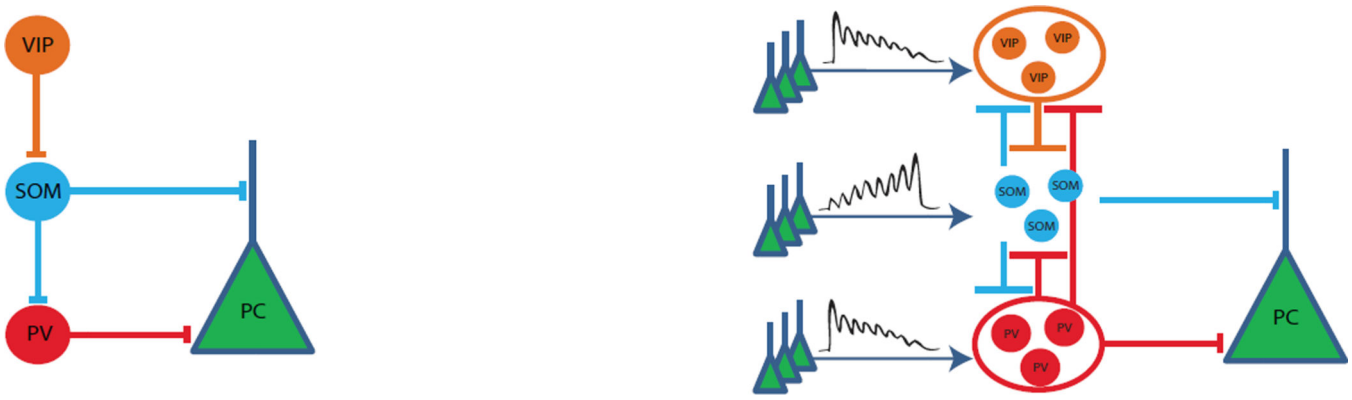

Figure 6. Connectivity schematics

Left, prevailing model of hierarchical interneuron connectivity in L2/3 based on (Hangya et al., 2014, Harris and Shepherd, 2015, Kepecs and Fishell, 2014, Pfeffer et al., 2013, Zhang et al., 2014, Lee et al., 2013). Right, proposed new cooperative model based on our findings and the above mentioned studies as well as others described in text.